ACS Photonics

Article

pubs.acs.org/journal/apchd5

Quantitative Extraction of Equivalent Lumped Circuit Elements for Complex Plasmonic Nanostructures

Banafsheh Abasahl, Christian Santschi, and Olivier J. F. Martin*

Nanophotonics and Metrology Laboratory (NAM), Swiss Federal Institute of Technology Lausanne (EPFL), 1015 Lausanne, Switzerland

Supporting Information

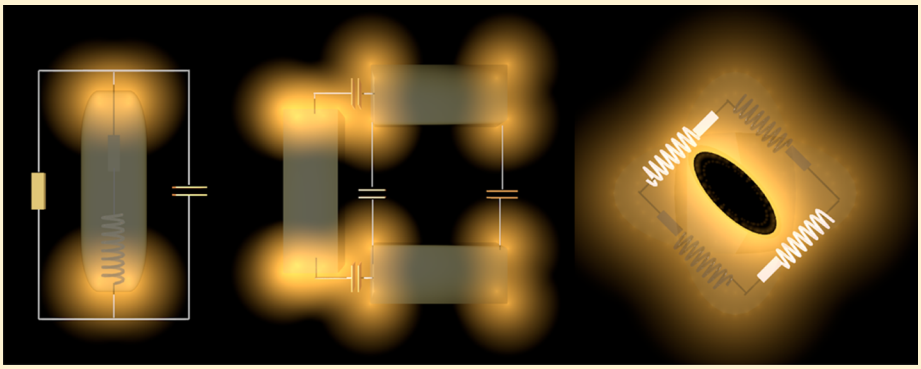

ABSTRACT: We establish a general method to bridge the gap between full-field electromagnetic calculations and equivalent lumped circuit elements to describe the optical response of plasmonic nanostructures. The exact value of each lumped element is extracted from one single full-field calculation using the Poynting vector and considerations on the energy flow in the system. The equivalent circuit obtained this way describes the complete response of the system at any frequency and can be used to optimize it for specific applications or perform parametric studies. This powerful approach can accurately reproduce the behavior of complex plasmonic nanostructures, such as Fano resonances, retardation effects, and polarization coupling. Furthermore, the influence of coupling parameters within the different modes supported by a given plasmonic structure can be investigated, thus providing new physical insights into its functioning mechanisms.

KEYWORDS: *circuit model, equivalent model, lumped elements, plasmonic structures, impedance matching*

Over the past decade, a broad variety of plasmonic nanostructures have been developed to localize light below the diffraction limit, enhance the electromagnetic near-field, or shape at will the optical spectrum.[1−6] These developments have been guided by a wealth of results produced with numerical techniques that can solve Maxwell's equations.[7−14] These full-field calculations can provide the response of a plasmonic nanostructure with great accuracy, usually for one given excitation condition. Yet, they do not provide much insight into the underlying mechanisms that lead to the observed response. To gain such insights, coupled oscillator models[15−22] or lumped circuit elements are far more useful.[23−29] They provide a figurative representation of the plasmonic system and facilitate its application-driven design and optimization. The harmonic oscillator approach combines masses and springs to mimic energy reservoirs and coupling. The parameters are subsequently extracted by fitting the response to full-wave calculations or to measured data. In a circuit approach, on the other hand, the values of the *RLC* elements (resistance *R*, inductance *L*, and capacitor *C*) are often derived using simplified models as suggested by Engheta and collaborators[23,26−28] and Greffet et al.[30] In the design of the transmission lines it is convenient to consider the different parts of the system as lumped circuit elements in order to arrange them for producing the desired characteristics and, subsequently, to replace each lumped element with its equivalent component of a transmission line.[31] Here, we show how the equivalent circuit approach can be brought a very significant step further by bridging the gap between lumped circuit elements and full-field calculations. We present the quantitative derivation of the equivalent circuit elements based on the electromagnetic field calculated using the surface integral (SI) method. From observables related to energy in the system and retrieved in the near-field and the far-field, we obtain the exact elements with respect to an excitation normalized to unity for the equivalent lumped circuit. The resulting equivalent circuit provides better insights into the functioning mechanisms of complex plasmonic nanostructures over the entire spectrum and accurately reproduces its response, including subtle effects such as polarization conversion. In addition, this powerful

Received: November 1, 2013
Published: April 2, 2014

approach can be used to design and efficiently optimize complex plasmonic systems with desired properties.

DEMONSTRATION OF THE MODEL AND EXTRACTION OF THE PARAMETERS

The optical response of a dipole antenna can be mimicked by an *RLC* circuit as shown in Figure 1a. In this approach, the

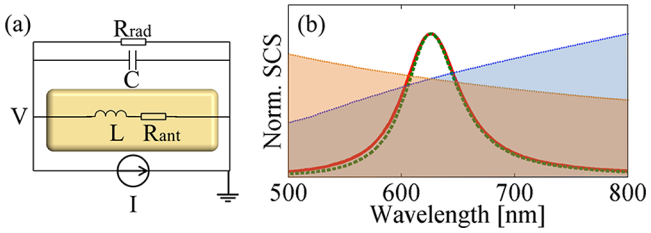

Figure 1. (a) Single dipole antenna with its equivalent lumped circuit elements and (b) the normalized far-field scattering cross-section calculated solving Maxwell's equations using a surface integral method (green dashed line) or the lumped circuit elements (red solid line). The two shadow areas correspond to energy storage in the capacitor (orange) and in the inductor (blue). The resonance occurs at $\lambda_0 = 627$ nm.

body of the antenna is considered as a wire with inductivity L and resistivity R_{ant}. Since the antenna losses are related to the electric current flowing through the resistor R_{ant} (representing the ohmic loss), it is wired in serial with the inductance L. On the other hand, the antenna couples to the surrounding medium through the capacitor C parallel to the $L-R_{ant}$ branch. In the visible range, plasmonic metals exhibit a negative real part of their permittivity that is lower than their surrounding dielectric; thus the electric field is confined to the vicinity of the structure and the surrounding of the antenna exhibits a capacitive behavior with capacity C. Radiative losses can be represented by a resistor R_{rad}, which is connected in parallel with the capacitor C. Using such an approach, the capacitor branch describes both the near- and far-field of the plasmonic mode.

In a lossless LC circuit at resonance frequency, where impedance matching between the inductive and capacitive branches is fulfilled, the energy oscillates between capacitor C and inductor L. Consequently, on average, the amount of energy stored in C and L is equal. However, real radiating antennas are lossy systems exhibiting radiative and nonradiative losses, which are represented by R_{rad} and R_{ant}, respectively. For a maximal radiation power at the resonance frequency ω_0, impedance matching of the capacitive branch, $Z_c = R_{rad}||1/j\omega C$ (where || means that the two impedances are connected in parallel), and inductive branch, $Z_L = R_{ant} + j\omega L$, must be satisfied. Therefore, the values of R_{ant} and R_{rad} can be determined from full-field calculations using the following procedure. The integral of the Poynting vector over the antenna surface represents the average power in the inductive branch, namely, the power stored inside the antenna, which at resonance frequency ω_0 is equal to the power in the capacitive branch, representing the energy outside of the antenna. Therefore, capacitor C and resistor R_{rad} can be extracted from the integral of the Poynting vector. The electric field, as shown in Figure 1a, providing the Poynting vector of a single elliptical antenna has been calculated using the surface integral method at a distance of 1 Å above the surface of the structure.[9] The integral of the Poynting vector over the entire surface provides the total power, the real part of which corresponds to loss in the antenna. As previously mentioned, at resonance frequency ω_0, the same power can be attributed to the radiative loss and to the capacitive storage. Separating the complex power into its real and imaginary parts, the values of the equivalent circuit elements in each branch can be extracted using eqs 1−4:

$$C = \frac{P^{i}}{|V|^2\omega_0} \tag{1}$$

$$R_{rad} = \frac{|V|^2}{P^{r}} \tag{2}$$

$$P^{r}R_{ant}{}^2 - |V|^2R_{ant} + \omega_0{}^2P^{r}L^2 = 0 \tag{3}$$

$$P^{i}\omega_0{}^2L^2 - \omega_0|V|^2L + P^{i}R_{ant}{}^2 = 0 \tag{4}$$

where P^r and P^i are real and imaginary parts of the power at resonance, respectively, and V is the voltage over the branches, as shown in Figure 1a. The derivation of eqs 1−4 is given in the Supporting Information. Hereinafter, the current amplitude I is assumed to be unity.

In addition to the shape of the structure, the optical properties of the metal strongly influence the response of the antenna. Since the permittivity ϵ, and therefore the field penetration depth into the metal, is dependent on the frequency, the corresponding L and R_{ant} must be determined for each frequency ω. Here, the skin depth $\delta(\omega)$ in the metal is assumed to be a measure for the current cross-section, i.e., for the resistivity. Hence, the values of L and R_{ant} at a given frequency ω can be obtained by dividing their values at resonance by $\delta(\omega)/\delta(\omega_0)$. Gold nanostructures are assumed throughout, and the values for ϵ are taken from ref 32.

The equivalent power P^r radiated by the antenna is dissipated into R_{rad} and shown for a dipole antenna of length 110, height 40, and width 40 nm in Figure 1b (red solid line). It is in very good agreement with the scattering cross-section obtained with the surface integral method (green dashed line). For this geometry, the circuit elements extracted using eqs 1−4 are C = 47 aF, L = 2.3 fH, R_{rad} = 59.02 Ω, and R_{ant} = 0.847 Ω. The shadow areas in Figure 1b represent the capacitive and inductive energy stored respectively in C and L, calculated from the equivalent circuit. They reveal that the system preferentially stores energy in the form of electric energy below the resonance and in the form of magnetice energy above the resonance. At resonance, the amount of electric and magnetic energy becomes equal, a signature of impedance matching, as was assumed initially. With these values, the time constants of the capacitive and the inductive branches are $\tau_C = R_{rad}C = 2.8210^{-15}$ s and $\tau_L = L/R_{ant} = 2.7210^{-15}$ s, which shows that the capacitive and the inductive branches have similar time constants. Let us emphasize that the approach developed here requires only one single full-field computation at the resonance frequency to retrieve the circuit elements; the response of the system at any other frequency is then obtained from the equivalent circuit.

CIRCUIT REPRESENTATION OF DOLMEN STRUCTURES

Using the circuit shown in Figure 1a as a building block, more complex systems can be investigated by cross-connecting the individual building blocks using appropriate coupling elements. For example, dolmen structures as shown in Figure 2a are well-

dx.doi.org/10.1021/ph400101w | ACS Photonics 2014, 1, 403−407

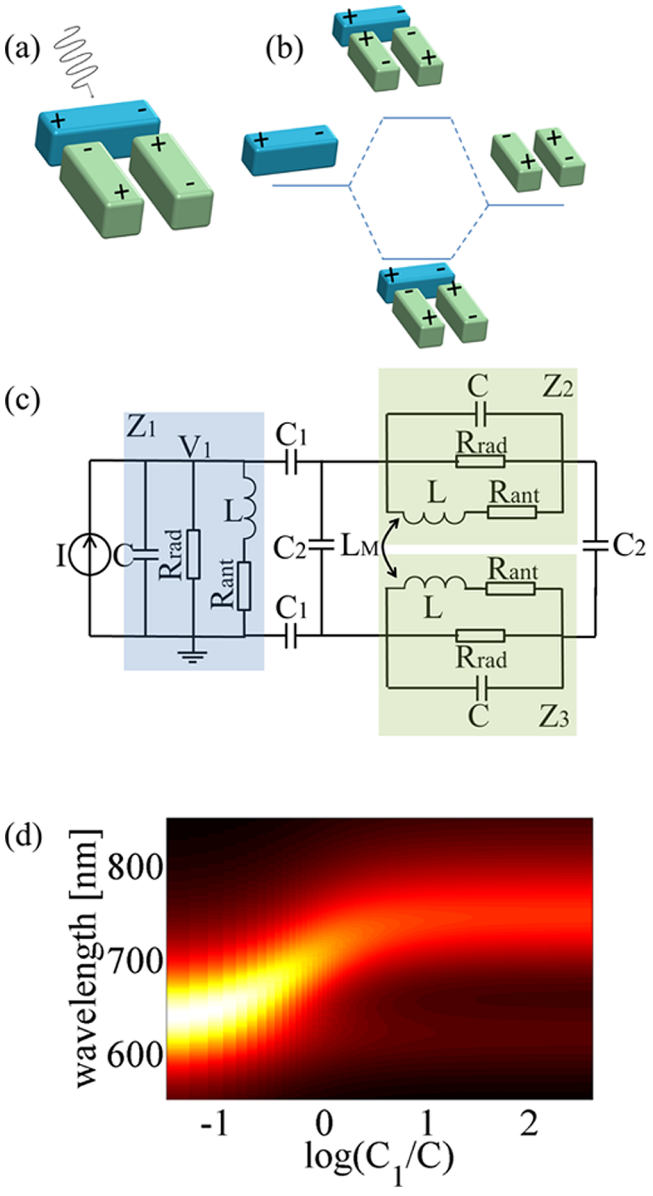

Figure 2. (a) Dolmen structure. The dipole shown in blue is excited by the incoming light, while the dipoles forming a quadrupole shown in green cannot be directly excited. (b) Hybridization diagram between the dipolar and quadrupolar modes. (c) Equivalent circuit model for the dolmen structure shown in (a). The elements in the blue and green building blocks belong to the corresponding dipoles in (a). (d) Scattering spectrum as a function of the perturbation introduced through C_1. The horizontal bar is the logarithmic scale of C_1/C, and the scattering intensity is normalized between 0 (black) and 1 (yellow).

known structures that exhibit Fano resonances.[33−36] The hybridization diagram for this type of structure is depicted in Figure 2b.[37] The transversal dipole (blue) can be excited from the far-field using an appropriate polarization. The parallel dipoles (green) are then excited via near-field coupling, resulting in a quadrupolar and nonradiative charge distribution near the Fano resonance wavelength.[35] As illustrated in Figure 2c, this configuration can be mimicked by a combination of three dipoles, Z_1, Z_2, and Z_3, two pairs of coupling capacitors, C_1 and C_2, and a mutual inductor L_M. The capacitor C_1, connecting Z_1 with Z_2 and Z_3, represents the capacitive coupling through the gaps. The capacitor C_2 describes the capacitive interaction between the orthostats represented by Z_2 and Z_3. The mutual inductor L_M represents the mutual magnetic effect of the two bars on each other. Note that the magnetic mutual coupling between Z_1 and the two other dipoles Z_2 and Z_3 can be neglected due to their respective dipole orientation.

In the dolmen structure shown in Figure 2a, changing the gap between the blue and the green elements changes the coupling and therefore the equivalent capacitor C_1. Figure 2d represents the response of the system as a function of a relative change of C_1 with respect to C, as a measure of the coupling strength between the bright mode of dipole Z_1 and the dark-quadrupolar mode of Z_2 and Z_3, which is represented by C_2. The response represents well the mode splitting due to the coupling between the transversal and parallel dipoles leading to a Fano resonance; see Figure 2d. Let us finally note that the data obtained from the circuit can be further used to fit additional models for the Fano resonance (see Supporting Information).

CIRCUIT REPRESENTATION OF CIRCULARLY POLARIZED ANTENNAS

We finally illustrate the utilization of quantitative equivalent circuits by considering a more complex plasmonic structure that can be used to generate circularly polarized light from a linearly polarized incident beam, Figure 3.[38] The structure is composed of two perpendicularly arranged elliptical antennas with a cavity at the center of the structure, Figure 3a. When this configuration is excited using an appropriate linear polarization, the polarization of the scattered light is converted into a left- or right-handed circular polarization state, through the superposition of two spatially and temporally orthogonal modes. The strength of this conversion is determined by the asymmetry of the cavity, Figure 3a and c. Since the configuration in Figure 3a is symmetric upon linear excitation along the x-axis, only linearly polarized light along the x-direction can be reradiated and the dipole along the y-axis cannot be excited. Full-wave calculations were performed on this system, and the corresponding circuit elements extracted at the resonance wavelength. Note that the energy level of the x-oriented antenna is affected by the presence of the arms pointing in the y-direction, although the y-oriented dipole cannot be excited.

This structure can be decomposed into two dipoles in the x- and y-direction, with four equal inductive paths, namely, M and m, between them, Figure 3b. Since the coupling is caused by the motion of the electrons in the metal, nonradiative resistances R_M and R_m are also included in these paths.

The equivalent circuit of the asymmetric structure is shown in Figure 3d. In the case of the symmetric structure in Figure 3a, the yellow and blue paths of the circuit are equal and voltages V_2 and V_3 become equal, and hence the voltage on the y-oriented part (pink color) is zero; therefore no coupling occurs from the x-oriented dipole to the y-oriented one. Consequently no energy is transferred to the y-oriented dipole, which becomes obsolete, and the circuit can be simplified as shown in Figure 3e. In order to extract the values corresponding to the inductors L and the resistors R_{ant} of these paths, the structure is divided into two parts, indicated with blue and green shadows in Figure 3d. While the values of C and R_{rad} are extracted with respect to the total power, requiring integration of the Poynting vector over the entire surface of the structure, the values of L and R_{ant} are extracted from the power in the pink and green regions, and the values of

dx.doi.org/10.1021/ph400101w | ACS Photonics 2014, 1, 403−407

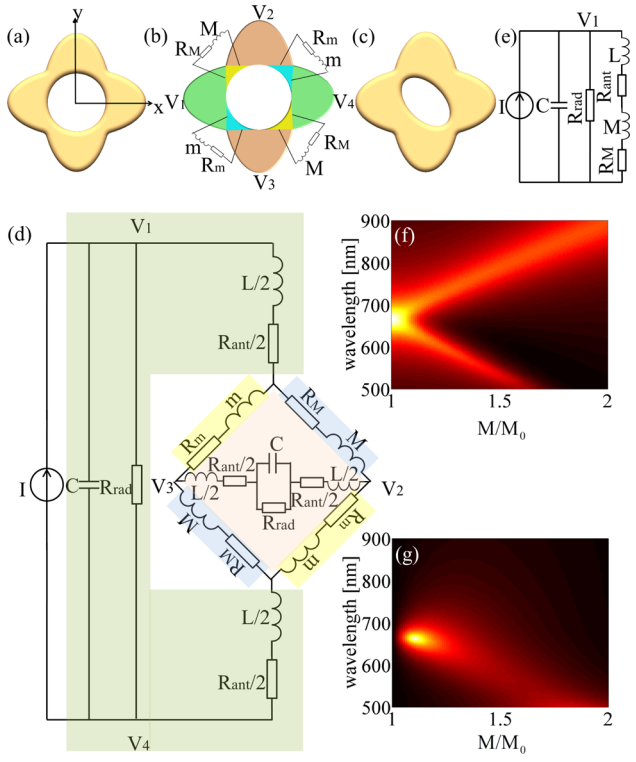

Figure 3. (a) Symmetric structure made of two orthogonal ellipses with a circular hole in the center. (b) The pink-green and blue-yellow regions correspond to the area where the integration of the Poynting vector is been performed for the calculation of the normal inductance and the coupling inductance, respectively. (c) Schematic of the system with a nonsymmetrical hole, which perturbs the system by coupling the two orthogonal ellipses, leading to a circular polarized response. (d) Equivalent circuit model for (c). (e) Simplified circuit of the symmetric system (a). (f) Scattering cross-section and (g) degree of circular polarization obtained upon introducing the nonsymmetrical hole, leading to a coupling between both ellipses.

M, m, R_M, and R_m are extracted from the power in the yellow and blue regions. Note that in the case of the symmetric structure $M = m$ and $R_M = R_m$. Upon introducing an elliptical asymmetric cavity in the structure, the blue and yellow paths become unbalanced, and consequently the energy can couple to the branch corresponding to the y-oriented part of the antenna. The dimensions of the structure and the extracted values for the circuit elements are provided in the Supporting Information. Figure 3f shows the scattering cross-section with respect to the power dissipated in the far-field resistors R_{rad} upon changing the values of M and m. The sum $M + m$ is equal to $2M_0$, where M_0 corresponds to the unperturbed system. In Figure 3f we present the scattering cross-section of the system as a function of the amount of perturbation applied on M. This figure clearly shows the mode-splitting associated with the strong coupling regime.

The circular polarization factor α_c is defined as

$$\alpha_c = \frac{|C_{right}| - |C_{left}|}{|C_{right}| + |C_{left}|} \tag{5}$$

where C_{left} and C_{right} are the left- and the right-handed circular polarization coefficients of the decomposition into the two orthogonal polarizations. The values $\alpha_c = +1$, $\alpha_c = -1$, and $\alpha_c = 0$ correspond to completely right-handed circular polarization, completely left-handed circular polarization, and linear polarization, respectively. Since the voltages $V_1 - V_4$ and $V_2 - V_3$ correspond to the voltage drop on the x- and y-oriented antennas, the coefficients can be extracted using the following equations:

$$C_{right} = |(V_1 - V_4) - j(V_2 - V_3)| \tag{6}$$

$$C_{left} = |(V_1 - V_4) + j(V_2 - V_3)| \tag{7}$$

Figure 3g shows the absolute value of α_c for different perturbations. The value is very low when the perturbation (and hence the coupling) is weak. With increasing perturbation α_c approaches 1. By further increasing the perturbation, i.e., in the strong coupling regime, this value drops again. This behavior is in perfect agreement with the full-field calculations reported in ref 38.

CONCLUSION

We have proposed a general method to bridge the gap between full-field electromagnetic calculations and equivalent lumped circuit elements to describe the optical response of plasmonic nanostructures. The exact value of each lumped element is extracted by considering the impedance matching between the capacitive branch and the inductive branch of the circuit, corresponding to the energy stored in the surrounding medium or in the antenna itself, respectively. It has been shown that this approach provides a very powerful method for extracting numerical values of all the lumped elements describing a complex plasmonic system. In turn, the extracted equivalent circuit can be used to optimize the response of the system without performing heavy full-field electromagnetic calculations at every frequency. As examples, the lumped elements associated with plasmonic structures supporting several dipolar modes, such as dolmen and time-retarded structures, have been retrieved. This powerful approach can accurately reproduce behavior of complex plasmonic circuits, including Fano resonances, retardation effects, and polarization coupling. Furthermore, the influence of coupling parameters within the different modes supported by these structures can be investigated. This approach provides a useful alternative to the oscillator model, since each block in the circuit relates to a specific geometrical part of the system, therefore providing straightforward correspondence.

ASSOCIATED CONTENT

Supporting Information

Extraction of the matching equations, dimensions, and extracted parameters for the dolmen and circularly polarized antennas and Fano resonance fitting. This material is available free of charge via the Internet at http://pubs.acs.org.

AUTHOR INFORMATION

Corresponding Author

*E-mail: olivier.martin@epfl.ch. Phone: +41 (0)21 69 32607. Fax: +41 (0)21 69 32614.

Notes

The authors declare no competing financial interest.

ACKNOWLEDGMENTS

This work was supported by the Swiss National Science Foundation (NCCR Nanoscale Science, projects 200021-125326 and CR23I2-147279).

REFERENCES

(1) Barnes, W. L.; Dereux, A.; Ebbesen, T. W. Surface plasmon subwavelength optics. *Nature* **2003**, *424*, 824.
(2) Hutter, E.; Fendler, J. H. Exploitation of localized surface plasmon resonance. *Adv. Mater.* **2004**, *16*, 1685−1706.
(3) Maier, S. A. *Plasmonics: Fundamentals and Applications*; Spinger-Verlag: Berlin, 2007.
(4) Giannini, V.; Fernndez-Domnguez, A.; Sonnefraud, Y.; Roschuk, T.; Fernndez-Garca, R.; Maier, S. A. Controlling light localization and light matter interactions with nanoplasmonics. *Small* **2010**, *6*, 2498−2507.
(5) Atwater, H. A.; Polman, A. Plasmonics for improved photovoltaic devices. *Nat. Mater.* **2010**, *9*, 205−213.
(6) Novotny, L.; van Hulst, N. Antennas for light. *Nat. Photonics* **2011**, *5*, 83−90.
(7) Martin, O. J. F.; Dereux, A.; Girard, C. Iterative scheme for computing exactly the total field propagating in dielectric structures of arbitrary shape. *J. Opt. Soc. Am. A Opt. Image. Sci. Vis.* **1994**, *11*, 1073−1080.
(8) Kottmann, J. P.; Martin, O. J. F. Accurate solution of the volume integral equation for high-permittivity scatterers. *IEEE Trans. Antennas Propag.* **2000**, *48*, 1719−1726.
(9) Kern, A. M.; Martin, O. J. F. Surface integral formulation for 3D simulations of plasmonic and high permittivity nanostructures. *J. Opt. Soc. Am. A* **2009**, *26*, 732−740.
(10) des Francs, G. C.; Grandidier, J.; Massenot, S.; Bouhelier, A.; Weeber, J. C.; Dereux, A. Integrated plasmonic waveguides: A mode solver based on density of states formulation. *Phys. Rev. B* **2009**, *80*, 7.
(11) McMahon, J. M.; Henry, A. I.; Wustholz, K. L.; Natan, M. J.; Freeman, R. G.; Van Duyne, R. P.; Schatz, G. C. Gold nanoparticle dimer plasmonics: finite element method calculations of the electromagnetic enhancement to surface-enhanced Raman spectroscopy. *Anal. Bioanal. Chem.* **2009**, *394*, 1819−1825.
(12) Chen, Y. T.; Nielsen, T. R.; Gregersen, N.; Lodahl, P.; Mork, J. Finite-element modeling of spontaneous emission of a quantum emitter at nanoscale proximity to plasmonic waveguides. *Phys. Rev. B* **2010**, *81*.
(13) Teulle, A.; Marty, R.; Viarbitskaya, S.; Arbouet, A.; Dujardin, E.; Girard, C.; des Francs, G. C. Scanning optical microscopy modeling in nanoplasmonics. *J. Opt. Soc. Am. B* **2012**, *29*, 2431−2437.
(14) Hohenester, U.; Trgler, A. MNPBEM A Matlab toolbox for the simulation of plasmonic nanoparticles. *Comput. Phys. Commun.* **2012**, *183*, 370−381.
(15) Gallinet, B.; Martin, O. J. F. Ab initio theory of Fano resonances in plasmonic nanostructures and metamaterials. *Phys. Rev. B* **2011**, *83*, 235427.
(16) Alzar, C. L. G.; Martinez, M. A. G.; Nussenzveiga, P. Classical analog of electromagnetically induced transparency. *Am. J. Phys.* **2001**, *70*, 4.
(17) Mukherjee, S.; Sobhani, H.; Lassiter, J. B.; Bardhan, R.; Nordlander, P.; Halas, N. J. Fanoshells: Nanoparticles with Built-in Fano Resonances. *Nano Lett.* **2010**, *10*, 2694−2701.
(18) Rahmani, M.; Lukiyanchuk, B.; Ng, B.; Tavakkoli, A.; Liew, Y. F.; Hong, M. H. Generation of pronounced Fano resonances and tuning of subwavelength spatial light distribution in plasmonic pentamers. *Opt. Express* **2011**, *19*, 4949−4956.
(19) Joe, Y. S.; Satanin, A. M.; Kim, C. S. Classical analogy of Fano resonances. *Phys. Scr.* **2006**, *74*, 259−266.
(20) Kats, M. A.; Yu, N.; Genevet, P.; Gaburro, Z.; Capasso, F. Effect of radiation damping on the spectral response of plasmonic components. *Opt. Express* **2011**, *19*, 21748−21753.
(21) Liu, N.; Langguth, L.; Weiss, T.; Kastel, J.; Fleischhauer, M.; Pfau, T.; Giessen, H. Plasmonic analogue of electromagnetically induced transparency at the Drude damping limit. *Nat. Mater.* **2009**, *8*, 758−762.
(22) Novotny, L. Strong coupling, energy splitting, and level crossings: A classical perspective. *Am. J. Phys.* **2010**, *78*, 1199−1202.
(23) Engheta, N. Circuits with light at nanoscales: Optical nanocircuits inspired by metamaterials. *Science* **2007**, *317*, 1698−1702.
(24) Iizuka, H.; Engheta, N.; Fujikawa, H.; Sato, K. Arm-edge conditions in plasmonic folded dipole nanoantennas. *Opt. Express* **2011**, *19*, 12325−12335.
(25) Polemi, A.; Alu, A.; Engheta, N. Nanocircuit loading of plasmonic waveguides. *IEEE Trans. Antennas Propag.* **2012**, *60*, 4381−4390.
(26) Alu, A.; Salandrino, A.; Engheta, N. Coupling of optical lumped nanocircuit elements and effects of substrates. *Opt. Express* **2007**, *15*, 13865−13876.
(27) Liu, N.; Wen, F.; Zhao, Y.; Wang, Y.; Nordlander, P.; Halas, N. J.; Al, A. Individual nanoantennas loaded with three-dimensional optical nanocircuits. *Nano Lett.* **2012**, *13*, 142−147.
(28) Engheta, N.; Salandrino, A.; Alu, A. Circuit elements at optical frequencies: Nanoinductors, nanocapacitors, and nanoresistors. *Phys. Rev. Lett.* **2005**, *95*.
(29) Agio, M.; Alu, A. *Optical Antennas*; Cambridge University Press: Cambridge, 2013; Vol. *1*, p 374.
(30) Greffet, J. J.; Laroche, M.; Marquier, F. Impedance of a nanoantenna and a single quantum emitter. *Phys. Rev. Lett.* **2010**, *105*.
(31) Clarricoats, R.; Rahmat-Samii, Y.; Wait, J. *Handbook of Microstrip Antennas*; Peter Peregrinus Ltd.: London, United Kingdom, 1989; Vol. *1*.
(32) Christy, P. B. J.; W, R. Optical constants of transition metals: Ti, V, Cr, Mn, Fe, Co, Ni, and Pd. *Phys. Rev. B* **1974**, *9*, 15.
(33) Zhang, S.; Genov, D. A.; Wang, Y.; Liu, M.; Zhang, X. Plasmon-induced transparency in metamaterials. *Phys. Rev. Lett.* **2008**, *101*.
(34) Verellen, N.; Sonnefraud, Y.; Sobhani, H.; Hao, F.; Moshchalkov, V. V.; Van Dorpe, P.; Nordlander, P.; Maier, S. A. Fano resonances in individual coherent plasmonic nanocavities. *Nano Lett.* **2009**, *9*, 1663−1667.
(35) Gallinet, B.; Martin, O. J. F. Relation between near-field and far-field properties of plasmonic Fano resonances. *Opt. Express* **2011**, *19*, 22167−22175.
(36) Francescato, Y.; Giannini, V.; Maier, S. A. Plasmonic systems unveiled by Fano resonances. *ACS Nano* **2012**, *6*, 1830−1838.
(37) Prodan, E.; Radloff, C.; Halas, N. J.; Nordlander, P. A hybridization model for the plasmon response of complex nanostructures. *Science* **2003**, *302*, 419−422.
(38) Abasahl, B.; Dutta-Gupta, S.; Santschi, C.; Martin, O. J. F. Coupling strength can control the polarization twist of a plasmonic antenna. *Nano Lett.* **2013**, *13*, 4575−4579.